DALTON

Stabilization of cobalt(I) by the tripodal ligands tris(2-pyridyl)methane and tris(2-pyridyl)phosphine. Structural, spectroscopic and *ab initio* studies of the $[CoL_2]^{n+}$ species†

Kenneth R. Adam,[a] Peter A. Anderson,[a] Timothy Astley,[b] Ian M. Atkinson,[a] John M. Charnock,[c,d] C. David Garner,[d] Jacqueline M. Gulbis,[e] Trevor W. Hambley,[f] Michael A. Hitchman,[b] F. Richard Keene*,[a] and Edward R. T. Tiekink[e]

[a] *Department of Chemistry and Chemical Engineering, School of Molecular Sciences, James Cook University of North Queensland, Townsville, Queensland 4811, Australia*
[b] *Department of Chemistry, University of Tasmania, Hobart, Tasmania 7001, Australia*
[c] *CCLRC Daresbury Laboratory, Warrington WA4 4AD, UK*
[d] *Department of Chemistry, University of Manchester, Manchester M13 9PL, UK*
[e] *School of Chemistry, University of Sydney, Sydney, NSW 2001, Australia*
[f] *Department of Chemistry, University of Adelaide, Adelaide, South Australia 5005, Australia*

The nature of bonding in a series of complexes $[CoL_2]^{n+}$ [L = the tripodal ligand tris(2-pyridyl)methane or tris(2-pyridyl)phosphine, n = 1–3] has been investigated by single-crystal X-ray diffraction, X-ray absorption and electronic spectroscopy and density functional theory *ab initio* calculations. The structural studies reveal that the cobalt ions each exist in a distorted octahedral geometry defined by six N-donor atoms; the cations are all centrosymmetric. In both series of complexes the bond lengths Co^{I}–N ≈ Co^{II}–N > Co^{III}–N. Data from the various studies indicate that the 'cobalt(I)' state of the complex $[Co\{X(C_5H_4N\text{-}2)_3\}_2]^+$ (X = CH or P) is better described by the d^8 cobalt(I)–ligand formulation rather than as d^7 cobalt(II)–ligand radical.

The co-ordination compounds of chelating π-acceptor ligands such as bipy = 2,2′-bipyridine, phen = 1,10-phenanthroline and their analogues have been widely studied, particularly with regard to their photochemistry,[1] redox characteristics[2–4] and the stabilization of low metal oxidation states. In the last context the species $[Co(bipy)_3]^+$ has attracted considerable attention[3–6] because of its utility as a homogeneous reduction catalyst for the production of H_2 from H_2O,[7–9] CO from CO_2[10–12] and the reduction of organic substrates.[13,14] The nature of the ligand–metal interaction has been probed by electronic spectral,[15,16] magnetic moment,[16,17] NMR contact shift[18,19] and structural studies[2,6] aimed at elucidating whether the species is better described as an octahedral high-spin cobalt(I) d^8 system with substantial $Co(d_\pi)\rightarrow bipy(\pi^*)$ back donation, or alternatively as a cobalt(II) species containing a reduced $bipy^-$ ligand radical. The consensus resides with the former option. In particular, the high-spin d^8 configuration is in accord with the magnetic susceptibility values of 2.53[16] and 2.89 μ_B,[17] which compare with that found for the isoelectronic high-spin d^8 $[Ni(bipy)_3]^{2+}$, μ_{eff} = 2.88 μ_B.[20] Further, the VIS/near-IR spectrum of $[Co(bipy)_3]^+$ contains bands consistent with metal-to-ligand-charge transfer (m.l.c.t.) transitions, which Kaizu *et al.*[16] interpret as evidence that the electron furnished by reduction of $[Co(bipy)_3]^{2+}$ resides primarily on the central cobalt atom. Fitzgerald *et al.*[19] investigated NMR contact shifts in $[Co(bipy)_3]^+$, $[Co(dmbipy)_3]^+$, $[Ni(bipy)_3]^{2+}$ and $[Ni(dmbipy)_3]^{2+}$ (dmbipy = 4,4′-dimethyl-2,2′-bipyridine) on the basis that π-back bonding affects charge distribution, so that such effects would be expected to be exhibited in local changes in ^1H and ^{13}C NMR spectra.[18,21] It was shown that both σ- and

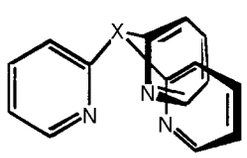

π-delocalization mechanisms were operative in $[Co(bipy)_3]^+$, and that the dominant π-delocalization mechanism most likely involved a direct overlap of the metal σ_{2e} orbitals with the highest-filled π-symmetry ligand orbitals, although other plausible mechanisms placing negative spin density in empty π* orbitals of the ligand were not discounted.[19]

Finally, the crystal structural investigation of Szalda *et al.*[6] compared the structures of the cobalt(I) complex $[Co(bipy)_3]^+$ and its high-spin cobalt(II) d^7 $[Co(bipy)_3]^{2+}$ analogue. The similarity of the Co–N bond lengths for the cobalt-(II) (average Co–N 2.128 Å) and -(I) complexes (average Co–N 2.11 Å) is in contrast with the large difference between the cobalt-(II) and -(III) species [1.93(2) Å].[22] In addition, a shortening of the bridging C(2)–C(2′) bond lengths in the bipy ligands was observed for the reduced form (1.42 *cf.* 1.49 Å). These data were interpreted to indicate that on reduction of the species from Co^{II} to Co^{I} the extra electron enters a d_π orbital and is partially delocalized *via* $Co(d_\pi)\rightarrow bipy(\pi^*)$ back donation. The trends in the Co–N distances in the $[Co(bipy)_3]^{n+}$ cations have also been observed in extended X-ray absorption fine structure (EXAFS) studies.[2]

The tripodal compounds $X(C_5H_4N\text{-}2)_3$ (X = N, CH, COH, P, P=O or As) and their complexes raise interesting questions with regard to the rationale described above. Boggess and Zatko[23,24] reported that the ligands with X = P and As stabilized Co^{I} whereas there was no stabilization when X = N: they attributed this observation to the ability of the bridging atom to allow delocalization throughout the ligand *via* p_π–d_π interaction between the bridgehead atom X and the pyridine rings, a mech-

† *Supplementary data available* (No. SUP 57201, 4 pp.): normalized Co K-edge EXAFS spectra of complexes involved in this study and table of radial distribution of atoms about the central Co atom. See Instructions for Authors, *J. Chem. Soc., Dalton Trans.*, 1997, Issue 1.

Non-SI units employed: $\mu_B \approx 9.27 \times 10^{-24}$ J T^{-1}, eV ≈ 1.60×10^{-19} J.

anism which is only possible for the larger bridgehead atoms. However, our re-examination of the electrochemistry of the cobalt complexes for X = N, COH, CH, P or P=O showed that in all cases the $[CoL_2]^+$ species were stabilized.[25] In that work we proposed that either the geometry imposed by the bridgehead atom allowed 'through space' delocalization between the rings, or that the orientation of the pyridyl rings in their constrained co-ordination geometries permitted enhanced overlap between the ligand p_π and the metal t_{2g} orbitals.

The specific mechanism of delocalization has implications for our general understanding of the nature of the interaction of polypyridyl ligands, such as 2,2′-bipyridine, with metal centres. The present study is directed at elucidating the metal–ligand interaction between Co^{I} and $X(C_5H_4N\text{-}2)_3$ (X = CH or P) using structural and spectroscopic techniques, and density functional theory (DFT) *ab initio* calculations which together provide an insight into the charge distribution in the complexes $[Co\{CH(C_5H_4N\text{-}2)_3\}_2]^+$ and $[Co\{P(C_5H_4N\text{-}2)_3\}_2]^+$.

Experimental

Materials

The following reagents were used as supplied without further purification: $Co(NO_3)_2{\cdot}6H_2O$ (Aldrich; 99+%), 2.2′-bipyridine (Merck, 99.5%), lithium perchlorate (Fluka, purum >98%), potassium hexafluorophosphate (Aldrich, 98%), tetra-*n*-butylammonium bromide (Fluka, 99%), tetraethylammonium bromide (Sigma) and silver nitrate (Aldrich, 99.9999%). Tetra-*n*-butylammonium hexafluorophosphate used in electrochemical measurements, was obtained from Fluka (puriss) and recrystallized twice from ethanol–water and twice from dichloromethane–diethyl ether. Acetonitrile (Aldrich, 99.9+%, HPLC grade) was used as received. Solvents used in the electrosynthesis and crystal growth of $[Co\{X(C_5H_4N\text{-}2)_3\}_2]^+$ [*viz.* diethyl ether, ethanol and light petroleum (b.p. 40–60 °C)] were rigorously purified using literature methods.[26]

Physical measurements

Electrochemistry. All electrochemical experiments were undertaken in a Vacuum Atmosphere glove-box under an argon atmosphere, using a Bioanalytical Systems BAS 100A electrochemical analyser. For cyclic voltammetry, solutions of the $[Co\{X(C_5H_4N\text{-}2)_3\}_2]^{n+}$ complexes (0.5–3 mmol dm^{-3}) were prepared in acetonitrile with $NBu^n_4PF_6$ (0.1 mol dm^{-3}) as the supporting electrolyte. A platinum-button working electrode, platinum-wire auxiliary and a $Ag–Ag^+$ reference electrode [0.01 mol dm^{-3} $AgNO_3$, 0.1 mol dm^{-3} $NBu^n_4PF_6$ in MeCN, +0.31 V *vs.* saturated calomel electrode (SCE)] were used. A sweep rate of 100 mV s^{-1} was used for cyclic voltammetry.

Electron absorption spectra. Single-crystal and potassium bromide disc electronic spectra were measured using a Cary 17 or 5 spectrophotometer fitted with a CTI Cryogenics unit, a Palm Beach 4025 cryogenic thermometer/controller or Oxford DTC2 temperature controller. Solutions of cobalt(I) complexes [(3–30) × 10^{-5} mol dm^{-3}] were prepared in ethanol under inert conditions, and their electronic spectra measured using a Cary 17 spectrophotometer.

Extended X-ray absorption fine structure. Samples used for X-ray absorption spectroscopy were ground with boron nitride using a mortar and pestle, and mounted in aluminium sample cells with Sellotape windows. The air-sensitive cobalt(I) samples were handled in a glove-box, and upon removal were immediately immersed in liquid nitrogen. Cobalt K-edge X-ray absorption spectra were recorded at ambient temperature for cobalt(II) and -(III) species, but at *ca.* 77 K for the cobalt(I) species which were mounted on the cold-finger of a liquid-nitrogen-filled cryostat in an evacuated sample chamber. The data were collected on Station 7.1 of the Daresbury Synchrotron Radiation Source, operating at 2 GeV with an average current of 150 mA. The data were analysed, including multiple scattering from the pyridine rings fixed at the geometry determined by crystallographic studies of these complexes by varying the shell distances and Debye–Waller parameters using EXCURV 92[27] to obtain optimum agreement between the experimental and simulated EXAFS and their Fourier transforms.

Syntheses

Tris(2-pyridyl)methane and tris(2-pyridyl)phosphine were obtained by literature methods.[28]

Bis[tris(2-pyridyl)methane]cobalt(II) nitrate, $[Co\{CH(C_5H_4N\text{-}2)_3\}_2][NO_3]_2$. A solution of $Co(NO_3)_2{\cdot}7H_2O$ (145 mg, 0.5 mmol) in acetone (5 cm^3) was added dropwise to a stirred solution of tris(2-pyridyl)methane (250 mg, 1.01 mmol) in acetone (10 cm^3). The resulting suspension was cooled at 0 °C for 2 h, the solid filtered off, washed with acetone and air dried. Yield: 260 mg, 76% (based on an anhydrous product).‡ Orange crystals of $[Co\{CH(C_5H_4N\text{-}2)_3\}_2][NO_3]_2$ were obtained by vapour diffusion of diethyl ether into an acetonitrile solution of the complex.

For use in the synthesis of $[Co\{CH(C_5H_4N\text{-}2)_3\}_2]Br$, the nitrate salt was converted into the hexafluorophosphate by metathesis from an aqueous solution with NH_4PF_6. The hexafluorophosphate salt was converted into the bromide by metathesis in an acetone solution using tetra-*n*-butylammonium bromide.

Bis[tris(2-pyridyl)phosphine]cobalt(II) nitrate, $[Co\{P(C_5H_4N\text{-}2)_3\}_2][NO_3]_2$. This complex was prepared in an analogous manner to the $[Co\{CH(C_5H_4N\text{-}2)_2\}_2][NO_3]_2$: yield 270 mg, 76% (based on an anhydrous product).‡ Orange crystals of $[Co\{P(C_5H_4N\text{-}2)_3\}_2][NO_3]_2{\cdot}8H_2O$ were obtained by slow evaporation of an aqueous solution of the complex.

Bis[tris(2-pyridyl)methane]cobalt(III) perchlorate, $[Co\{CH(C_5H_4N\text{-}2)_3\}_2][ClO_4]_3$. This complex was obtained by coulometry of a solution of $[Co\{CH(C_5H_4N\text{-}2)_3\}_2][NO_3]_2$ (*ca.* 50 mg) in HCl (0.1 mol dm^{-3}, 50 cm^3) at a platinum-gauze electrode at a potential of 0.50 V *vs.* an SCE reference electrode until the current decreased to <1% of its initial value. The resultant solution was reduced to a small volume and the complex precipitated by the addition of $LiClO_4$, filtered off, washed with ethanol and air dried. The yield was quantitative.‡ The perchlorate salt was converted into the bromide by anion-exchange chromatography. Yellow crystals of $[Co\{CH(C_5H_4N\text{-}2)_3\}_2]Br_3{\cdot}14H_2O$ were obtained by slow evaporation of an aqueous solution.

Bis[tris(2-pyridyl)phosphine]cobalt(III) perchlorate, $[Co\{P(C_5H_4N\text{-}2)_3\}_2][ClO_4]_3$. This complex was prepared by coulometry as described for $[Co\{CH(C_5H_4N\text{-}2)_3\}_2][ClO_4]_3$, at a potential of 0.70 V *vs.* SCE. The yield was quantitative.† Yellow crystals of $[Co\{P(C_5H_4N\text{-}2)_3\}_2][ClO_4]_3{\cdot}0.5H_2O$ were obtained by the slow evaporation of an aqueous solution.

Bis[tris(2-pyridyl)methane]cobalt(I) bromide, $[Co\{CH(C_5H_4N\text{-}2)_3\}_2]Br$. The electrosynthesis of $[Co\{CH(C_5H_4N\text{-}2)_3\}_2]Br$

‡ For this series of complexes considerable variation in the extent of hydration was experienced which rendered microanalysis difficult. In all cases but one, *viz.* $[Co\{P(C_5H_4N\text{-}2)_3\}_2]^+$, the salt ultimately obtained was characterized unambiguously by X-ray crystallography. In the latter case the established identity of the cobalt(II) precursor, the observation that its electrochemical characteristics were identical to those of the cobalt(II) species, and the close analogy with the $CH(C_5H_4N\text{-}2)_3$ counterpart were taken as sufficient verification of the assignment.

Table 1 Crystallographic data and refinement details for complexes **1**–**5**

	1	**2**	**3**	**4**	**5**
Formula	$C_{32}H_{54}Br_3CoN_6O_{14}$	$C_{32}H_{26}CoN_8O_6$	$C_{32}H_{28}BrCoN_6O$	$C_{30}H_{28}Cl_3CoN_6O_{14}P_2$	$C_{30}H_{40}CoN_8O_{14}P_2$
M	1045.46	677.5	651.4	923.8	857.6
Crystal size/mm	0.25 × 0.11 × 0.32	0.08 × 0.19 × 0.32	0.20 (dia.)	0.16 × 0.20 × 0.21	0.44 × 0.65 × 0.65
Colour	Orange	Orange	Blue	Orange-red	Red-orange
Crystal system	Orthorhombic	Trigonal	Orthorhombic	Orthorhombic	Monoclinic
Space group	*Pccn*	$R\bar{3}$	*Pbcn*	*Pccn*	*C*2/*c*
a/Å	21.183(6)	11.6572(7)	8.369(1)	12.634(2)	20.50(3)
b/Å	20.551(4)	11.6572(7)	19.714(1)	19.066(1)	11.00(1)
c/Å	11.480(2)	17.893(1)	19.145(4)	15.348(2)	16.83(2)
β/°					92.1(1)
U/Å^3	4997(2)	2116.4(5)	3159(1)	3697(1)	3793(8)
Z	4	3	4	4	4
D_c/g cm^{-3}	1.390	1.595	1.370	1.660	1.501
F(000)	2128	1047	1328	1880	1780
μ/cm^{-1}	28.27	6.75	17.9	8.44	6.13
Absorption correction	Numerical	Empirical	—	Analytical	Empirical
Transmission factors	0.525–0.748	0.957–1.029	—	0.766–0.900	0.900–1.028
Diffractometer	CAD4F	AFC6R	CAD4F	CAD4F	AFC6R
No. of data collected	3909	1239	2414	2791	3792
θ_{max}/°	23.0	27.5	22.5	22.5	25.0
No. unique data	3909	1123	2065	2430	3679
No. unique data [with $I \geqslant n\sigma(I)$]	1308 (2.5)	950 (3.0)	709 (2.5)	1502 (2.5)	2983 (3.0)
R	0.072*	0.041	0.063	0.040	0.048
R′	0.063*	0.049	0.065	0.057	0.059
Residual electron density/e Å^{-3}	0.4	1.26	1.26	0.36	0.70

* $R = \Sigma(||F_o| - |F_c||)/\Sigma|F_o|$, $R' = [\Sigma w(|F_o| - |F_c|)^2/\Sigma wF_o^2]^{\frac{1}{2}}$.

was carried out in an inert (Ar) atmosphere. The complex $[Co\{CH(C_5H_4N\text{-}2)_3\}_2]Br_2$ (*ca.* 50 mg) was dissolved in dry ethanol–acetonitrile (5:2, 7 cm^3) and electrolyte added (NBu^n_4Br, 20 mg, producing a solution *ca.* 0.01 mol dm^{-3}). The complex was reduced coulometrically at a platinum-gauze working electrode in a three-compartment cell using an Ag–Ag$^+$ reference electrode (0.01 mol dm^{-3} $AgNO_3$). The electrolysis was conducted at −1.55 V (*vs.* Ag–Ag$^+$) over 2 h, during which time the orange solution changed to a deep blue with precipitation of a dark solid. The electrolyte solution in the platinum-auxiliary electrode side-arm was changed at regular intervals throughout the electrolysis. When the cell current had dropped to a steady value (<5% of the initial current) the product was filtered off and washed with ethanol–diethyl ether (1:3 v/v) and then diethyl ether (×3). Yield: *ca.* 20 mg.‡ Dark blue crystals suitable for structural analysis were obtained by liquid diffusion of diethyl ether into a solution of the complex in dry ethanol. A single crystal was isolated in a tapered glass capillary and sealed with the exclusion of air.

Bis[tris(2-pyridyl)phosphine]cobalt(I) perchlorate, $[Co\{P(C_5H_4N\text{-}2)_3\}_2]ClO_4$. The electrosynthesis of $[Co\{P(C_5H_4N\text{-}2)_3\}_2]ClO_4$ was carried out in a similar manner to that described for $[Co\{CH(C_5H_4N\text{-}2)_3\}_2]Br$. The complex $[Co\{P(C_5H_4N\text{-}2)_3\}_2][NO_3]_2$ (*ca.* 18 mg, 0.025 mmol) was dissolved in acetronitrile–dry ethanol (4:3, 8 cm^3) containing $LiClO_4$ as electrolyte (*ca.* 0.015 mol dm^{-3}). The electrolysis was conducted at −1.40 V (*vs.* Ag–Ag$^+$) over 3 h, during which the initially orange solution changed to a deep blue and the cell current had dropped to less than 2% of the initial value. The electrolysis solution was shaken with light petroleum (30 cm^3) giving rise to a blue layer of reduced volume (predominantly MeCN) and a clear layer (light petroleum and EtOH). Upon separation of the solvent layers, diethyl ether (20 cm^3) was added to the blue layer causing the precipitation of the blue product, which was filtered off and washed with diethyl ether.‡ Despite many attempts, no crystals were obtained which provided satisfactory X-ray diffraction for determination of the structure by crystallography.

Ab initio calculations

Density functional theory calculations were performed on an SGI Power Challenge computer system using the GAUSSIAN 94 package.[29] The local spin-density approximation (LSDA) S-VWN5[30] exchange-correlation potential was used in this work together with the 3-21G basis set, which was the largest practical with our computational facilities. This corresponded to 401, 423 and 427 basis functions for $[Co(bipy)_3]^{n+}$, $[Co\{CH(C_5H_4N\text{-}2)_3\}_2]^{n+}$ and $[Co\{P(C_5H_4N\text{-}2)_3\}_2]^{n+}$ (n = 1–3) systems, respectively.

The bonding analysis was based on the Mulliken population overlap scheme[31,32] where electron overlaps are distributed between the atoms involved. Mulliken population overlaps give fractional electron occupancies which can yield useful information regarding bond strengths, despite not being normalized to integral values. Total atomic charges are calculated as the difference between the atomic number and the gross atomic population. Despite the shortcomings of Mulliken analysis the scheme has been widely used for determining atomic charges within molecules.[33–35]

Owing to the computational expense of the optimization of the geometries of the complexes, only single-point calculations were performed using the coordinates taken from the available crystal structures. In the case of $[Co\{P(C_5H_4N\text{-}2)_3\}_2]^+$ where an X-ray determination was not available the coordinates used were those of $[Co\{P(C_5H_4N\text{-}2)_3\}_2]^{2+}$. This approximation is justified by the apparent similarity between the structures of the two complexes observed from the EXAFS data.

X-Ray crystallography

The crystallographic data are summarized in Table 1, and selected interatomic parameters for the five structures are given in Table 2.

$[Co\{CH(C_5H_4N\text{-}2)_3\}_2]Br_3\cdot 14H_2O$ 1. Cell constants were determined by a least-squares fit to the setting parameters of 25 independent reflections, measured and refined on an Enraf-Nonius CAD4-F diffractometer fitted with a graphite monochromator. Data were obtained at 21 °C with Mo-Kα radiation (λ = 0.710 69 Å).

The structure was solved by heavy-atom methods using SHELXS 86[36] and the solution was extended by Fourier-

Table 2 Selected bond lengths (Å) and angles (°) for complexes **1**–**5**

	1 X = C	**2** X = C	**3** X = C	**4** X = P	**5** X = P
Co–N(11)	1.95(1)	2.109(2)	2.09(1)	1.967(4)	2.096(3)
Co–N(21)	1.95(1)		2.13(1)	1.984(4)	2.121(3)
Co–N(31)	1.95(1)		2.12(2)	1.978(4)	2.108(4)
N(11)–C(12)	1.36(2)	1.334(3)	1.31(2)	1.359(6)	1.322(4)
N(11)–C(16)	1.34(2)	1.330(3)	1.36(2)	1.347(6)	1.331(5)
N(21)–C(22)	1.33(2)		1.35(3)	1.355(7)	1.334(4)
N(21)–C(26)	1.37(2)		1.33(2)	1.359(6)	1.316(5)
N(31)–C(32)	1.33(2)		1.29(3)	1.349(7)	1.330(4)
N(31)–C(36)	1.32(2)		1.34(3)	1.352(6)	1.330(5)
X(1)–C(16)	1.50(2)	1.501(3)	1.51(2)	1.829(5)	1.808(4)
X(1)–C(26)	1.48(2)		1.51(3)	1.817(6)	1.821(4)
X(1)–C(36)	1.54(2)		1.52(3)	1.825(5)	1.821(4)
C(12)–C(13)	1.40(2)	1.356(4)	1.34(3)	1.360(7)	1.360(6)
C(13)–C(14)	1.37(2)	1.371(4)	1.39(3)	1.376(8)	1.350(6)
C(14)–C(15)	1.36(2)	1.363(4)	1.40(3)	1.369(8)	1.363(6)
C(15)–C(16)	1.34(2)	1.375(4)	1.40(3)	1.378(7)	1.373(5)
C(22)–C(23)	1.35(2)		1.34(3)	1.368(8)	1.367(5)
C(23)–C(24)	1.42(2)		1.39(4)	1.368(9)	1.345(7)
C(24)–C(25)	1.39(2)		1.39(3)	1.374(9)	1.356(6)
C(25)–C(26)	1.35(2)		1.42(3)	1.389(8)	1.371(5)
C(32)–C(33)	1.37(2)		1.38(4)	1.368(8)	1.360(5)
C(33)–C(34)	1.37(2)		1.32(4)	1.385(9)	1.332(6)
C(34)–C(35)	1.38(2)		1.38(4)	1.370(9)	1.360(5)
C(35)–C(36)	1.35(2)		1.43(3)	1.376(8)	1.346(5)
N(11)–Co–N(21)	88.4(4)	85.50(9)[a]	86.9(6)	91.5(2)	88.7(1)
N(11)–Co–N(31)	88.9(5)	85.50(9)[b]	86.6(6)	91.7(2)	89.3(1)
N(21)–Co–N(31)	89.6(5)	85.50(9)[a,b]	85.8(6)	91.6(2)	89.7(1)
N(11)–Co–N(21)	91.6(4)[c]	94.50(9)[d]	93.1(6)[e]	88.5(2)[f]	91.3(1)[e]
N(11)–Co–N(31)	91.1(5)[c]	94.50(9)[g]	93.4(6)[e]	88.3(2)[f]	90.7(1)[e]
N(21)–Co–N(31)	90.4(5)[c]	85.50(9)[d,g]	94.2(6)[e]	91.6(2)[e,f]	90.3(1)[e]
Co–N(11)–C(12)	121(1)	123.3(2)	125(1)	119.5(3)	120.6(3)
C(12)–N(11)–C(16)	119(1)	118.8(2)	117(1)	122.6(3)	121.5(2)
C(12)–N(11)–C(16)	119(1)	117.8(2)	118(2)	117.8(4)	117.9(3)
Co–N(21)–C(22)	123(1)		124(1)	119.4(3)	120.3(3)
Co–N(21)–C(26)	119(1)		117(1)	122.1(3)	121.5(2)
C(22)–N(21)–C(26)	118(1)		118(2)	118.6(4)	118.0(3)
Co–N(31)–C(32)	122(1)		127(1)	119.5(4)	120.4(3)
Co–N(31)–C(36)	121(1)		116(1)	121.8(3)	122.1(2)
C(32)–N(31)–C(36)	117(2)		116(2)	118.5(6)	117.4(3)
C(16)–X(1)–C(26)	109(1)	111.6(2)[a]	110(1)	97.5(2)	101.3(2)
C(16)–X(1)–C(36)	110(1)		109(1)	100.0(2)	101.8(2)
C(26)–X(1)–C(36)	111(1)		108(1)	96.9(2)	99.2(2)
N(11)–C(12)–C(13)	119(2)	123.3(3)	124(2)	122.6(6)	123.2(4)
N(11)–C(16)–X(1)	116(1)	116.8(3)	121(2)	121.0(4)	121.6(2)
N(11)–C(16)–C(15)	122(2)	122.1(3)	120(2)	121.6(5)	121.8(3)
C(15)–C(16)–X(1)	123(2)	121.1(3)	119(2)	117.3(4)	116.6(3)
N(21)–C(22)–C(23)	124(2)		124(2)	121.8(5)	122.6(4)
N(21)–C(26)–X(1)	116(1)		121(2)	121.0(4)	121.4(3)
N(21)–C(26)–C(25)	122(2)		121(2)	118.1(4)	116.8(3)
C(25)–C(26)–X(1)	123(2)		118(2)	120.9(5)	121.7(3)
N(31)–C(32)–C(33)	123(1)		125(2)	122.2(5)	122.9(4)
N(31)–C(36)–X(1)	115(1)		121(2)	121.4(4)	120.6(3)
N(31)–C(36)–C(35)	124(2)		120(2)	120.9(5)	117.5(3)
C(35)–C(36)–X(1)	121(2)		119(2)	117.7(4)	121.9(3)
C(12)–C(13)–C(14)	122(2)	118.5(3)	122(2)	119.2(6)	118.9(4)
C(13)–C(14)–C(15)	117(2)	119.2(3)	114(2)	119.0(5)	119.2(3)
C(14)–C(15)–C(16)	122(2)	119.1(3)	122(2)	119.8(5)	119.0(4)
C(22)–C(23)–C(24)	118(2)		120(2)	119.9(6)	119.0(4)
C(23)–C(24)–C(25)	119(2)		117(2)	119.1(6)	118.9(4)
C(24)–C(25)–C(26)	120(2)		119(2)	119.6(5)	119.8(4)
C(32)–C(33)–C(34)	118(2)		122(2)	119.8(6)	118.7(4)
C(33)–C(34)–C(35)	119(2)		115(2)	117.7(6)	119.4(4)
C(34)–C(35)–C(36)	119(2)		122(2)	120.9(6)	119.7(4)

Symmetry operations: [a] $1 - y, -1 + x - y, z$; [b] $2 - x + y, 1 - x, z$; [c] $1 - x, -y, -z$; [d] $1 + y, 1 - x + y, 2 - z$; [e] $-x, -y, -z$; [f] $-x, 1 - y, 1 - z$; [g] $x - y, -1 + x, 2 - z$.

difference methods. Many peaks were found in the space between the cationic complexes. Only two of these could be unequivocally assigned as being bromide sites, and even they were only partially occupied. The remaining contribution to the 1.5 bromide anions expected could not be discerned from among the many oxygen(water) sites. Hydrogen atoms were included at calculated sites (C–H 0.95 Å) with fixed isotropic thermal parameters and all other atoms, with the exception of minor solvent or anion sites, were refined anisotropically. Full-matrix least-squares methods were used for the refinement (on F) of an overall scale factor, positional and thermal parameters. Neutral atom scattering factors were taken from

Cromer and Waber.[37] Anomalous dispersion effects were included in F_c;[38] the values for $\Delta f'$ and $\Delta f''$ were those of Creagh and McAuley.[39] The values for the mass-attenuation coefficients were those of Creagh and Hubbell.[40] All calculations were performed using the TEXSAN[41] crystallographic software package and plots were drawn using ORTEP.[42]

$[Co\{CH(C_5H_4N\text{-}2)_3\}_2][NO_3]_2$ 2, $[Co\{CH(C_5H_4N\text{-}2)_3\}_2]Br\cdot H_2O$ 3, $[Co\{P(C_5H_4N\text{-}2)_3\}_2][ClO_4]_3\cdot 2H_2O$ 4 and $[Co\{P(C_5H_4N\text{-}2)_3\}_2][NO_3]_2\cdot 8H_2O$ 5. Intensity data for complexes **2**–**5** were measured at room temperature (20 °C) on an Enraf-Nonius CAD4F (**3** and **4**) or a Rigaku AFC6R diffractometer (**2** and **5**) fitted with graphite-monochromated Mo-Kα radiation (λ = 0.710 73 Å) employing the ω–2θ scan technique in each case. The data sets were corrected for Lorentz-polarization effects and an absorption correction was applied for **2**,[43] **3**[43] and **4**.[44]

The structures were solved by placing the metal cation at an appropriate site of symmetry and were each refined (**3** and **4**;[44] **2** and **5**[41]) by a full-matrix least-squares procedure based on *F*. Non-H atoms were refined with anisotropic thermal parameters and H atoms included in the models in their calculated positions (C–H 0.97 Å); the water H atoms were not located in the refinements of complexes **3**–**5**. The refinements were continued until convergence employing a weighting scheme of the form $[\sigma^2(F) + g|F|^2]^{-1}$ for **3** ($g = 0.008$)[44] and **4** ($g = 0.002$)[44] and sigma weights $[1/\sigma^2(F)]$[41] for **2** and **5**. The analysis of variance showed no special features indicating that an appropriate weighting scheme had been applied in each case; no corrections were applied for extinction effects. The numbering schemes employed for **4** and **5** are available as supplementary material. All figures are drawn with ORTEP[42] using 25% probability ellipsoids. The SHELX 76[44] program was employed for the analysis of **3** and **4** and TEXSAN[41] for **2** and **5**.

Complex **1** consists of cations, disordered Br^- anions and approximately fourteen water molecules. The structure is made up of the hydrophobic cations in a close-packed arrangement with an unusually extensive solvent/anion layer occupying the intervening space, as shown in Fig. 4. In this respect the crystals resemble those of a protein and behave similarly; *i.e.* if the crystals are exposed to air for more than a few seconds they become opaque and do not diffract X-rays. Two of the solvent/anion sites could be assigned as partially occupied bromide, amounting to approximately one bromide. The remaining 0.5 bromide in the asymmetric unit could not be located and one or more of the sites assigned as oxygen must in fact be a bromide. On this basis it is estimated that there are seven water molecules comprising the asymmetric unit. Mobility and disorder of the solvent/anion atoms severely limited the quality and extent of the diffraction data and, as a consequence, a detailed analysis of the derived interatomic parameters is inappropriate.

Atomic coordinates, thermal parameters and bond lengths and angles have been deposited at the Cambridge Crystallographic Data Centre (CCDC). See Instructions for Authors, *J. Chem. Soc., Dalton Trans.*, 1997, Issue 1. Any request to the CCDC for this material should quote the full literature citation and the reference number 186/324.

Results and Discussion

X-Ray crystallography

The structures of the bis(ligand) cobalt complexes of tris(2-pyridyl)methane in three different formal oxidation states have been determined, as well as those of the analogous cobalt-(II) and -(III) complexes of tris(2-pyridyl)phosphine. The structures of a number of cobalt complexes of other tripodal π-acceptor ligands have been reported previously: for the cobalt(III) complexes of tris(2-pyridyl)amine[45] and tris(2-pyridyl)methanol,[46] and the cobalt(II) complex of tris(pyrazol-1-yl)methane.[47]

The molecular structures of the cations in complexes **1**–**5** are shown in Figs. 1–3 and as supplementary material, and selected interatomic parameters are collected in Table 2; details of anion/solvent geometries and intermolecular associations of interest for **2**–**5** have been deposited. In the structures of **1** and **3**–**5** the cobalt atom is located on a crystallographic centre of inversion and in **2** the metal is located at a site of symmetry $\bar{3}$. The cations each feature a slightly distorted N_6 octahedral geometry with the octahedral faces being defined by the nature of the bridgehead atom X in the tripodal ligands $X(C_5H_4N\text{-}2)_3$ where X = CH or P.

As has been noted recently,[48] coherent series of related structures are still relatively rare despite the availability of modern techniques. This arises, in part, because of the difficulty of obtaining suitable crystals for X-ray crystallographic analyses. In the present investigation structures for complexes **1**–**5** have been obtained, although their analysis has been less than optimal. Significant experimental difficulties were encountered with the diffraction study (see Experimental section) and hence, while the cation structures have been determined unambiguously, there are relatively high errors associated with the derived interatomic parameters in some of the structures, thereby making general comparisons of ligand parameters difficult. Nevertheless, it is still possible to determine with a measure of confidence the magnitude of the Co–N interactions as the oxidation state is changed. Thus, in the $CH(C_5H_4N\text{-}2)_3$ series the average Co–N interactions vary from 1.95(1) to 2.109(2) to 2.111(7) Å for the cobalt-(III), -(II) and -(I) complexes, respectively; *i.e.* a significant increase from Co^{III} to Co^{II} but no apparent increase from Co^{II} to Co^{I}. For the $P(C_5H_4N\text{-}2)_3$ complexes, for which the estimated standard deviations are significantly lower, the average Co–N distance in the cobalt(III) complex of 1.976(2) Å compares with 2.108(2) Å in the cobalt(II) analogue. As the Co–N distances lengthen there is a widening in the Co–N(*n*1)–C(*n*2) angles ($n = 1$–3) and a concomitant decrease in the Co–N(*n*1)–C(*n*6) angles, particularly for the **1**–**3** series. Given the limitations of the data it is only possible to compare the geometric parameters for the ligands in **2** and **5** [monitoring the effect on the cobalt(II) centre as X is varied from CH to P] and between **4** and **5** (examining the effect when the oxidation state of cobalt is changed).

Comparing the structures of complexes **2** and **5**, *i.e.* changing X from CH to P in the cobalt(II) complexes, the average Co–N bond distances of 2.109(2) and 2.108(2) Å, respectively, are indistinguishable. This similarity is extended to the N–C (ring) bond distances which average 1.332(2) and 1.328(2) Å, respectively, and indeed the C–C distances. The most significant difference in the cations is found in the parameters involving the X atom, *i.e.* the expected increase in X–C and a contraction of the angles (*ca.* 10°) about the X atom in **5**. From this analysis it can be concluded that the cobalt and pyridine parameters are largely independent of the nature of X.

Comparing the two $P(C_5H_4N\text{-}2)_3$ structures with the cobalt-(II) and -(III) centres, some systematic changes in the ligand parameters are noted mirroring the changes in the Co–N bond distances. As the Co–N bond distances increase in complex **5** the average N–C(ring) distances decrease, *i.e.* 1.328(2) Å for **5** *cf.* 1.354(3) Å for **4**. Even allowing for the greater errors in the C–C parameters in the pyridine rings, the C–C distances in **5** are longer than the comparable distances in **4**. Clearly, there is an influence on the ligand parameters as the oxidation state of the cobalt cation is varied.

EXAFS Studies

Extended X-ray absorption fine structure beyond an X-ray absorption edge arises from back scattering of the ejected photoelectron by atoms adjacent to the absorbing atom.[49,50] The intensity and frequency of the EXAFS may be interpreted in terms of the number, nature and distance of the back-scattering atoms adjacent to the absorbing atom,[50–52] and in

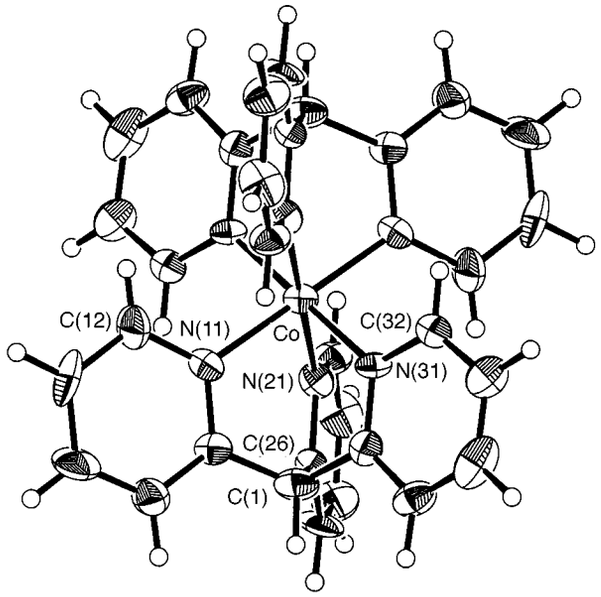

Fig. 1 Molecular structure and crystallographic numbering scheme for the cation in $[Co\{CH(C_5H_4N\text{-}2)_3\}_2]Br_3\cdot 14H_2O$ **1**

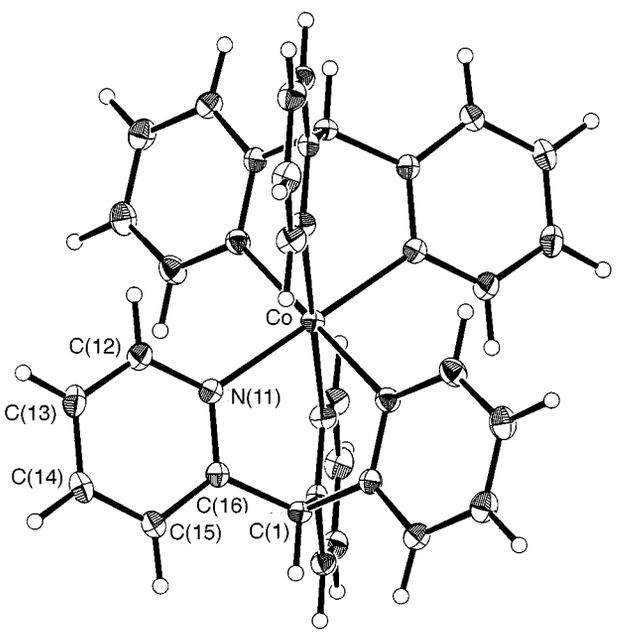

Fig. 2 Molecular structure and crystallographic numbering scheme for the cation in $[Co\{CH(C_5H_4N\text{-}2)_3\}_2][NO_3]_2$ **2**

addition the edge position in the normalized near-edge spectra is indicative of the oxidation state.[53]

In the current study of the $[Co\{X(C_5H_4N\text{-}2)_3\}_2]^{n+}$ complexes structural data from the EXAFS measurements provide information complementary to the X-ray crystallographic results. The environment of the central cobalt atoms has been investigated in each complex. This allows a direct comparison of the Co–N distances obtained by cobalt K-edge EXAFS with those determined by X-ray crystallography, and in the case of $[Co\{P(C_5H_4N\text{-}2)_3\}_2]^+$ (where suitable crystals proved elusive) the cobalt K-edge EXAFS provides the only available measurement of the Co–N distances within this complex and allows other predictions regarding its likely structure to be made. Such comparisons have been made previously for the $[Co(bipy)_3]^{n+}$ system.[2,6]

The cobalt K-edge positions and cobalt-ligand distances determined by X-ray absorption spectroscopy are presented in Table 3. There is a clear shift to lower energy in edge position in going from Co^{III} to Co^{II}, with a corresponding increase in the

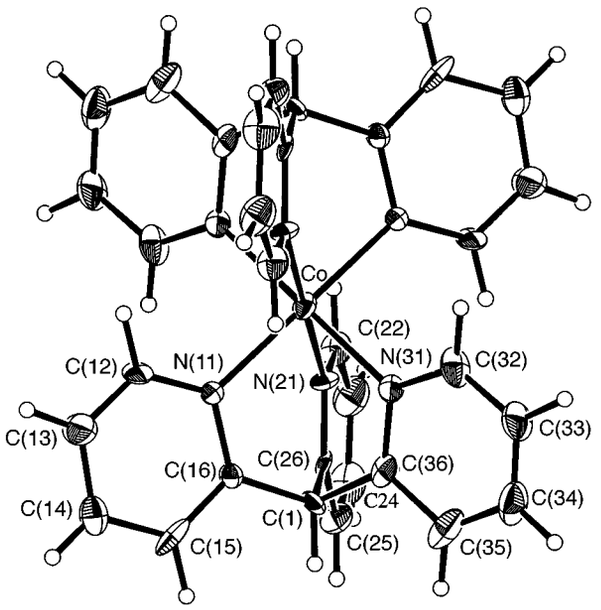

Fig. 3 Molecular structure and crystallographic numbering scheme for the cation in $[Co\{CH(C_5H_4N\text{-}2)_3\}_2]Br\cdot H_2O$ **3**

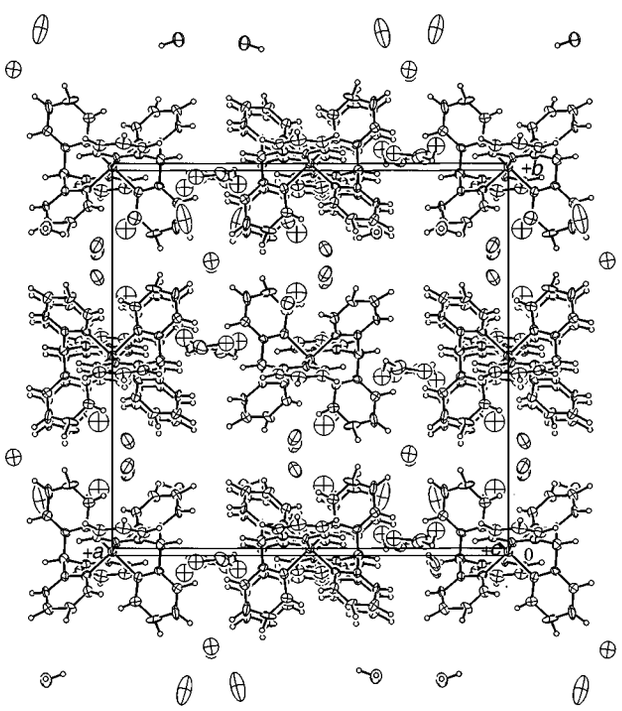

Fig. 4 Packing diagram for complex **1** showing close-packed cations with an intervening solvent–anion layer

Table 3 The K-edge positions (E_0) and Co–N distances as determined by EXAFS and single-crystal X-ray diffraction

		Co–N/Å	
Complex[a]	E_0/eV	EXAFS[b]	X-Ray[c]
$[Co\{CH(C_5H_4N\text{-}2)_3\}_2][ClO_4]_3$	7718.4	1.94	—
$[Co\{CH(C_5H_4N\text{-}2)_3\}_2]Br_3$	—	—	1.95(1)
$[Co\{CH(C_5H_4N\text{-}2)_3\}_2][NO_3]_2$	7714.7	2.12	2.109(2)
$[Co\{CH(C_5H_4N\text{-}2)_3\}_2]Br$	7713.8	2.10	2.111(7)
$[Co\{P(C_5H_4N\text{-}2)_3\}_2][ClO_4]_3$	7718.2	1.97	1.976(2)
$[Co\{P(C_5H_4N\text{-}2)_3\}_2][NO_3]_2$	7714.5	2.13	2.108(2)
$[Co\{P(C_5H_4N\text{-}2)_3\}_2][ClO_4]$	7713.9	2.10	—

[a] Anions indicated, hydration omitted for simplicity. [b] The estimated uncertainty is ±0.03 Å. [c] Average values.

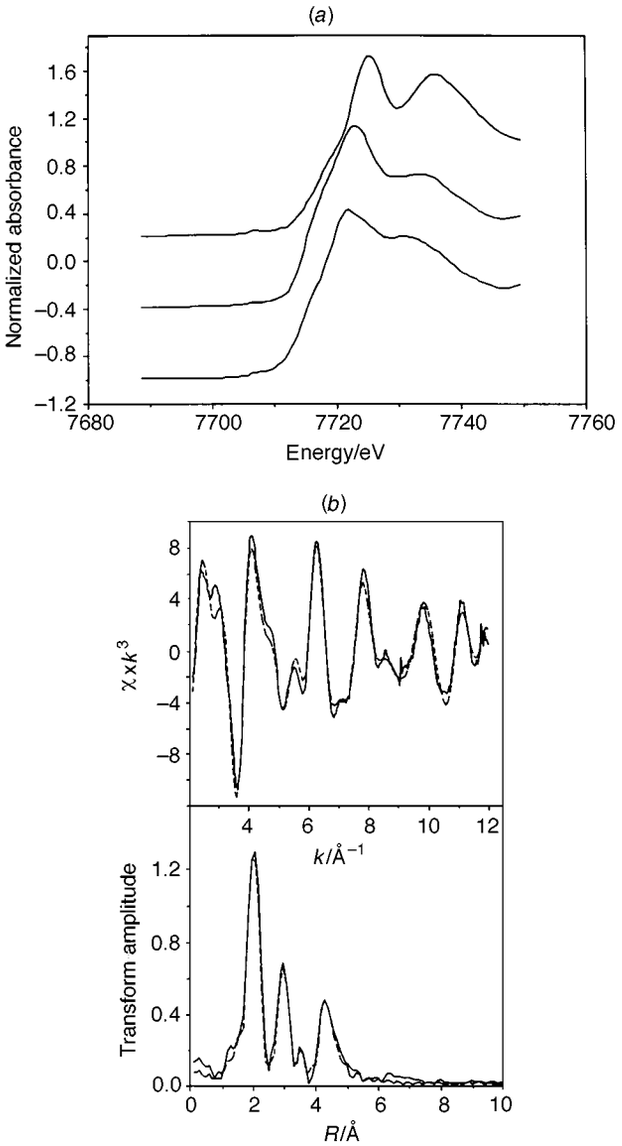

Fig. 5 (*a*) Normalized cobalt-edge XANES (X-ray absorption near-edge structure) profiles of $[Co\{P(C_5H_4N\text{-}2)_3\}_2][ClO_4]_3$ (top), $[Co\{P(C_5H_4N\text{-}2)_3\}_2][NO_3]_2$ and $[Co\{P(C_5H_4N\text{-}2)_3\}_2]ClO_4$ (bottom). (*b*) The EXAFS (top) and Fourier transform of $[Co\{P(C_5H_4N\text{-}2)_3\}_2]ClO_4$. ——, Experiment; – – –, simulation

Co–N bond length. However, there is no significant difference between the cobalt-(II) and -(I) complexes. The k^3-weighted cobalt K-edge EXAFS of $[Co\{P(C_5H_4N\text{-}2)_3\}_2]^{n+}$, together with its Fourier transform are shown in Fig. 5. The equivalent cobalt K-edge spectra for the other complexes have been deposited.

The structural information derived from the EXAFS and X-ray crystallographic determinations shows a high degree of agreement for each of the five complexes where both experiments were possible (Table 3). The EXAFS results confirm the trend in the $[Co\{CH(C_5H_4N\text{-}2)_3\}_2]^{n+}$ series where the bond lengths Co^{I}–N ≈ Co^{II}–N > Co^{III}–N. The radial distributions of the atoms about the central cobalt up to *ca.* 5 Å (see SUP 57201) are strikingly similar for the $[Co\{CH(C_5H_4N\text{-}2)_3\}_2]^{+}$ and $[Co\{CH(C_5H_4N\text{-}2)_3\}_2]^{2+}$ cations, and for the $[Co\{P(C_5H_4N\text{-}2)_3\}_2]^{+}$ and $[Co\{P(C_5H_4N\text{-}2)_3\}_2]^{2+}$ cations.

Analysis of the structural data cannot in itself answer the principal questions raised regarding the electronic nature of the $[Co\{X(C_5H_4N\text{-}2)_3\}_2]^{n+}$ complexes and the reason for the stabilization of the formally cobalt(I) state. However, such data do establish some very important points. First, the Co–N distance for both the $[Co\{CH(C_5H_4N\text{-}2)_3\}_2]^{n+}$ series is not significantly different for the formally Co^{I}–N and Co^{II}–N species, with the Co^{III}–N bond length substantially shorter. This is exactly analogous to the crystal structure results for the $[Co(bipy)_3]^{n+}$ series.[6] Secondly, if π-back bonding is operative in these systems, the α(C)-to-X (bridgehead) bond distance does not constitute an indicator for it, as there are no significant differences in this parameter for either system. Thirdly, the bridgehead atom imposes steric constraints on the orientation of the pyridine rings, and is responsible for variations in the N–Co–N bond angles and other angles between analogous complexes. Thus the bridgehead atom potentially influences the overlap of metal- and ligand-centred orbitals.

Apart from the obvious structural differences imposed by the oxidation state of the metal centre and the bridgehead atom X, the complexes are very similar with respect to overall geometry and intraligand bond distances and angles. The structural parameters of the pyridine rings in $[Co\{CH(C_5H_4N\text{-}2)_3\}_2]^{+}$ do show some differences to those in the cobalt-(II) and -(III) complexes. However, within the limitations imposed by the accuracy of the crystal structure determinations, it is not possible to identify any significant inequivalence of the pyridine rings in the $[Co\{CH(C_5H_4N\text{-}2)_3\}_2]^{+}$ structure.

The observed pattern of Co–N bond lengths may be considered from two perspectives. On the one hand, as the occupancy of the metal d orbitals varies: Co^{III}, low spin, $(t_{2g})^6$; Co^{II}, high spin, $(t_{2g})^5(e_g)^2$; Co^{I}, high spin, $(t_{2g})^6(e_g)^2$. Thus, the cobalt-(II) and -(I) configurations have two electrons in the Co–N σ-antibonding orbitals and would be expected to have not only bond lengths longer than that for the cobalt(III) situation but also a similar bond length, as the variation in the t_{2g} population is expected to have a lesser effect on the Co–N bond lengths.

The alternative interpretation is one of 'normal' Co^{III}–N and Co^{II}–N distances, and a short Co^{I}–N distance. Two possibilities arise. The $[Co\{X(C_5H_4N\text{-}2)_3\}_2]^{+}$ complexes may be described as $[Co^{II}\{X(C_5H_4N\text{-}2)_3\}\{X(C_5H_4N\text{-}2)_3^{\cdot -}\}]^{+}$ thus essentially containing Co^{II}–N bonds, or $[Co^{I}\{X(C_5H_4N\text{-}2)_3\}_2]^{+}$ with the unusually short Co^{I}–N bond due to significant π-back donation from the Co atom to the $X(C_5H_4N\text{-}2)_3$ ligands.

This issue was pursued by magnetic and spectroscopic studies, and the electronic nature of $[Co\{X(C_5H_4N\text{-}2)_3\}_2]^{+}$ has been investigated in the current study by *ab initio* calculations, as discussed below.

Electronic spectroscopy and bonding parameters

The electronic spectra of the cobalt-(II) and -(III) complexes were measured at 290 and ≈15 K as KBr discs, and the spectra of the cobalt(I) complexes were recorded as solutions in deaerated ethanol at 290 K. The spectrum of a crystal of $[Co\{CH(C_5H_4N\text{-}2)_3\}_2][PF_6]_2$ was also measured over the range 18 000–25 000 cm^{-1}.

For the ligand $CH(C_5H_4N\text{-}2)_3$, the cobalt(III) complex shows a broad peak centred at 23 000 cm^{-1} which can be assigned as the transition to the components of the $^1T_{1g}$ excited state, with absorption to charge transfer commencing at ≈27 000 cm^{-1}. A similar assignment has been reported[48] for the $CH(pz)_3$ (pz = pyrazolyl) complex, with the transition here occurring at 21 500 cm^{-1}. The higher band energy for the $CH(C_5H_4N\text{-}2)_3$ complex is in line with the bonding parameters derived for complexes of the mixed tripod ligand $CH(C_5H_4N\text{-}2)(pz)_2$, where pyridine was found to be a stronger ligand than pyrazole.[54]

The spectrum of the cobalt(II) complex is shown in Fig. 6(*a*) and consists of a peak at 11 800 cm^{-1} with a shoulder at 13 200 cm^{-1}, a weak sharp peak due to a spin-forbidden transition at 19 735 cm^{-1} and a broad peak centred at ≈23 100 cm^{-1} with a shoulder at ≈22 300 cm^{-1}. The first two transitions may safely be assigned to the $^4A_{1g}$ and ^4E_g states derived from the $^4T_{2g}$ level of the parent octahedral complex. The pair of peaks at *ca.* 23 000 cm^{-1} probably encompass the transitions to the $^4A_{2g}$ and ^4E_g states of the $^4T_{1g}$ level and the transition to the $^4A_{2g}(P)$ state which, as noted previously,[55] gives rise to a weak band which is

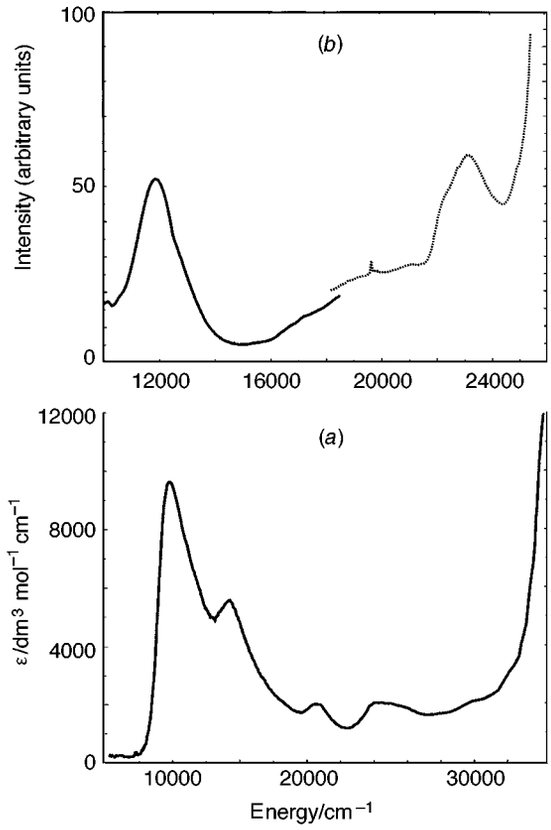

Fig. 6 The UV/VIS spectra of (*a*) $[Co\{CH(C_5H_4N\text{-}2)_3\}_2]^+$ (ethanol solution) and (*b*) $[Co\{CH(C_5H_4N\text{-}2)_3\}_2]^{2+}$ at 15 K [KBr disc and single crystal (···)]

often not resolved. The band energies and assignments are given in Table 4.

The solution spectrum of the $[Co\{CH(C_5H_4N\text{-}2)_3\}_2]^+$ species is shown in Fig. 6(*b*) and is dominated by a very intense peak at 9800 cm^{-1} ($\varepsilon = 10\,000$ dm^3 mol^{-1} cm^{-1}). This may be assigned as a metal-to-ligand charge-transfer transition, the low energy being consistent with the easy access of the cobalt(II) state, and the ready availability of low-energy empty π* orbitals on the ligand. A peak of moderate intensity occurs at 14 200 cm^{-1}, with a weaker band at 20 600 cm^{-1}, a weak broad band centred at ≈25 000 cm^{-1} and a very weak shoulder at ≈32 000 cm^{-1} on the edge of the intense absorption due to charge transfer and/or intraligand transitions. The assignment of the bands to 'd–d' transitions can only be tentative, since additional peaks may be masked under the intense charge-transfer band at 9800 cm^{-1}; moreover, it is possible that weak charge-transfer transitions may occur in this region. Three spin-allowed transitions are expected for the d^8-electron configuration of Co^{I} in an approximately octahedral ligand environment, and the bands at 14 200 and 20 600 cm^{-1} may be assigned to the transitions to the $^3T_{2g}$ and $^3T_{1g}(F)$ states, respectively. The transition to the $^3T_{1g}(P)$ state may then either give rise to the very weak peak at ≈32 000 cm^{-1} or be masked under the intense absorption commencing at ≈33 000 cm^{-1}. The weak broad band at ≈25 000 cm^{-1} is assigned to several spin-forbidden transitions which are expected in this region. The band energies and tentative assignments are summarized in Table 4.

Basically similar spectra were observed for the complexes of $P(C_5H_4N\text{-}2)_3$. That of the cobalt(III) complex shows a shoulder at ≈22 000 cm^{-1} which may be assigned to the 'd–d' transition to the $^1T_{1g}$ state, occurring on the edge of an intense charge-transfer absorption. The band energies and assignments of the cobalt-(II) and -(I) complexes are given in Table 4. Those of the cobalt(II) complex are very similar to those reported for the visible region by Holm *et al.*[56] for an acetonitrile solution of this complex (11 000 and 21 800 cm^{-1}) with the observation of additional weak peaks at 18 500 and 19 450 cm^{-1} in the present work assigned to spin-forbidden transitions. The intense metal-to-ligand charge-transfer occurs at slightly lower energy for $[Co\{P(C_5H_4N\text{-}2)_3\}_2]^+$ than for $[Co\{CH(C_5H_4N\text{-}2)_3\}_2]^+$ (8600 compared with 9800 cm^{-1}). A similar change has been observed for the iron(II) complexes of these ligands[57] where the corresponding bands occur at 21 500 and 22 800 cm^{-1}. The onset of the intense absorption in the ultraviolet also occurs at slightly lower energy in the $P(C_5H_4N\text{-}2)_3$ complex, ≈33 500 cm^{-1}.

For the cobalt(II) compounds metal–ligand bonding parameters were derived using the angular overlap model (AOM) by methods identical to those described previously for the analogous $CH(pz)_3$ and $CH(C_5H_4N\text{-}2)(pz)_2$[54] complexes. The calculated transition energies and associated bonding parameters are indicated in Table 4. Note that the π-bonding parameter refers to the out-of-plane interaction, the in-plane interaction being assumed negligible, as found in other studies.[47] The three sets of parameters for the $P(C_5H_4N\text{-}2)_3$ complex refer to the three different Co–N bond distances.[47,54] For both complexes, excellent agreement with the observed transition energies is obtained, the σ- and π-bonding parameters being very similar to those reported[54] for the pyridine group in $[Co\{CH(C_5H_4N\text{-}2)(pz)_2\}_2]^{2+}$ (e_σ ≈4575 cm^{-1}, $e_\pi = 930$ cm^{-1}), and quite similar to those of the pyrazole groups in $[Co\{CH(pz)_3\}_2]^{2+}$ (e_σ ≈4540 cm^{-1}, e_π ≈585 cm^{-1}).[47] Both $P(C_5H_4N\text{-}2)_3$ and $CH(C_5H_4N\text{-}2)_3$ thus act as quite strong σ donors and moderate π donors towards Co^{II}. The close similarity between the two sets of parameters implies that any conjugation across the bridgehead atom in the former ligand has an insignificant effect upon the π interaction with the metal.

Since the assignment of the 'd–d' transitions of the cobalt(I) compounds is only tentative any discussion of the bonding parameters in these complexes must be viewed with caution. If it is assumed that the peaks at ≈14 000 cm^{-1} correspond to the first transition of the cobalt(I) ion, calculated transition energies which are consistent with the spectrum observed for $[Co\{CH(C_5H_4N\text{-}2)_3\}_2]^+$ are obtained using an average σ-bonding parameter e_σ ≈4760 cm^{-1} with e_π close to zero. As in previous studies,[47,54] the e_σ values were scaled to take into account the different Co–N bond lengths observed in the solid complex, though it is possible that these differences are smaller in solution. The calculated splittings in each excited state are quite small, and consistent with the observed band widths. A significant non-zero value of e_π would be expected to produce resolvable band splittings similar to those observed for the analogous isoelectronic nickel(II) complexes.[47,58] The Racah parameter $B = 675$ cm^{-1} used in the calculations seems acceptable, representing a reduction to ≈77% of the value of 880 cm^{-1} estimated for the free cobalt(I) ion.[59] As the crystal structure of the $[Co\{P(C_5H_4N\text{-}2)_3\}_2]^+$ complex is unknown, analysis of the spectrum is less reliable. However, assuming a structure similar to that of the $[Co\{CH(C_5H_4N\text{-}2)_3\}_2]^+$ complex, which, except for the differences in the Co–N bond lengths, appears to be reasonable from an analysis of the EXAFS data, the transition energies may be reproduced satisfactorily using similar, though marginally smaller bonding and Racah parameters.

The above interpretation implies that the σ-bonding interaction in the cobalt(I) complexes is quite similar to that in the cobalt(II) complexes. This seems reasonable, as although the lower oxidation state will cause an expansion of the d orbitals, enhancing overlap with the ligand orbitals, the concomitant increase in the energy separation between the metal and ligand σ-bonding orbitals will produce a decrease in the metal–ligand interaction energy. Apparently, the two effects approximately balance. The marked decrease in the π-donor capacity of the ligands when the metal is in the lower oxidation state also seems reasonable, as the metal t_{2g} orbitals will shift in energy away from the filled ligand π orbitals towards the empty ligand π* orbitals. The relatively high π-acceptor character of the ligand

Table 4 Calculated and observed transition energies (in cm^{-1}) of the complexes $[Co\{X(C_5H_4N\text{-}2)_3\}_2]^{n+}$ (X = CH or P; n = 1 or 2)

$[Co\{CH(C_5H_4N\text{-}2)_3\}_2]^+$		
Transition	Calculated	Observed
c.t.[a]		9 800
	13 600	
$^3A_{2g} \longrightarrow {}^3T_{2g}$[b]	14 300	14 200
	14 550	
	19 950	
$^3A_{2g} \longrightarrow {}^3T_{1g}$[b]	20 700	20 600
	21 200	
c		≈25 000
	31 650	
$^3A_{2g} \longrightarrow {}^3T_{1g}$[b]	31 800	32 000
	32 225	
Bonding and Racah parameters (cm^{-1})		
e_σ	4500, 4650, 5135	
$e_{\pi y}$	0	
$e_{\pi x}$	0	
B	675	

$[Co\{CH(C_5H_4N\text{-}2)_3\}_2]^{2+}$		
Transition	Calculated	Observed
$^4A_{2g} \longrightarrow {}^4A_{1g}$	11 620	11 800
$^4A_{2g} \longrightarrow {}^4E_g$	13 000	13 200
c		19 725
$^4A_{2g} \longrightarrow {}^4A_{1g}$	22 520	22 300
$^4A_{2g} \longrightarrow {}^4E_g$	22 920	23 100
	4850	
	950	
	0	
	810	

$[Co\{P(C_5H_4N\text{-}2)_3\}_2]^+$		
Transition	Calculated	Observed
c.t.[a]		8 600
	13 950	
$^3A_{2g} \longrightarrow {}^3T_{2g}$	14 000	14 025
	14 030	
	19 525	
$^3A_{2g} \longrightarrow {}^3T_{1g}$[b]	20 250	19 600
	20 375	
c		≈23 250
	30 925	
$^3A_{2g} \longrightarrow {}^3T_{1g}$[b]	31 050	≈29 500
	31 925	
	4700	
	0	
	0	
	625	

$[Co\{P(C_5H_4N\text{-}2)_3\}_2]^{2+}$		
Transition	Calculated	Observed
	10 800	
$^4A_{1g} \longrightarrow {}^4T_{2g}$	11 400	12 000
	12 800	
c		18 500
		19 450
	21 510	
$^4A_{1g} \longrightarrow {}^4T_{1g}$	21 600	21 800
	22 500	
	4400, 4600, 4700	
	890, 930, 960	
	0	
	740	

[a] Metal-to-ligand charge-transfer transition. [b] Assignment tentative, see discussion. [c] Spin-forbidden transition, several of which are predicted in this region.

Table 5 Electrochemical data for $[Co\{X(C_5H_4N\text{-}2)_3\}_2]^{n+}$ cations and $[Co(bipy)_3]^{n+}$ [25,46]

	$E_{\frac{1}{2}}$[a]/V	
Complex	Co^{III}–Co^{II}	Co^{II}–Co^{I}
$[Co(bipy)_3]^{n+}$	0.32	−1.01
$[Co\{N(C_5H_4N\text{-}2)_3\}_2]^{n+}$ [b]	0.35	−1.11
$[Co\{CH(C_5H_4N\text{-}2)_3\}_2]^{n+}$	0.22	−1.21
$[Co\{P(C_5H_4N\text{-}2)_3\}_2]^{n+}$	0.55	−0.97
$[Co\{OP(C_5H_4N\text{-}2)_3\}_2]^{n+}$	0.99	−0.75
$[Co\{COH(C_5H_4N\text{-}2)_3\}_2]^{n+}$	0.19	−1.17

[a] In acetonitrile–0.1 mol dm^{-3} $NBu^n_4PF_6$ solution; platinum-button working electrode; 298 K; scan rate 100 mV s^{-1}; reference, saturated sodium chloride calomel electrode (SSCE). [b] Propylene carbonate (4-methyl-1,3-dioxolan-2-one)–0.2 mol dm^{-3} $NBu^n_4PF_6$.

in the cobalt(I) complexes is in accord with the behaviour normally associated with aromatic amines.

The ligand-field-splitting parameter Δ is given by $3e_\sigma - 2e_\pi$ for an aromatic amine with negligible in-plane π bonding. Substitution of the appropriate values (Table 4) implies that Δ rises from ≈12 650 cm^{-1} for $[Co\{CH(C_5H_4N\text{-}2)_3\}_2]^{2+}$ to ≈14 200 cm^{-1} for $[Co\{CH(C_5H_4N\text{-}2)_3\}_2]^{+}$, with the increase being due entirely to the enhanced π-acceptor character of the ligand. It is generally observed that a decrease in oxidation state is accompanied by a marked *decrease* in Δ, as is indeed the case on going from $[Co\{CH(C_5H_4N\text{-}2)_3\}_2]^{3+}$, where $\Delta \approx 25\,000$ cm^{-1}, to $[Co\{CH(C_5H_4N\text{-}2)_3\}_2]^{2+}$. However, it has been suggested [60] that the dominant cause of the decrease in Δ associated with the change from Co^{II} to Co^{III} is the marked contraction in the metal–ligand bond length, from 2.109 to 1.95 Å in the present case. The present analysis appears to support this viewpoint, suggesting that, at least where low oxidation states are concerned, a decrease in oxidation state is not always accompanied by a decrease in Δ.

It must be stressed that the above analysis is only tentative. An acceptable fit to the observed transition energies may also be obtained if the first spin-allowed transition of $[Co\{CH(C_5H_4N\text{-}2)_3\}_2]^{+}$ is at ≈10 000 cm^{-1}, masked by the charge-transfer transition at 9800 cm^{-1}, with calculated energies of the $^3T_{1g}$ states then being at 14 200 and 22 000 cm^{-1}. This would imply a Δ value of ≈10 000 cm^{-1}, considerably lower than the 12 650 cm^{-1} for the corresponding cobalt(II) complex. However, a Racah *B* parameter of ≈470 cm^{-1} is required for this assignment, which seems an unacceptably large reduction from the free-ion value of 880 cm^{-1} for Co^{I}.

Electrochemical studies

The electrochemical data for the cobalt complexes of a number of tripod ligands and bipy are given in Table 5.[25,46] The potential of the Co^{II}–Co^{I} couple can be taken as a measure of the stability of the cobalt(I) state. The data indicate that the $[Co\{X(C_5H_4N\text{-}2)_3\}_2]^{+}$ cations are stabilized to an extent comparable to $[Co(bipy)_3]^{+}$. It is expected that the reduction potentials of the unbound ligands would vary to a much greater degree than the Co^{II}–Co^{I} couples, indicating significant metal involvement in the reduction of the complexes. Unfortunately, reliable $E_{\frac{1}{2}}$ values for the ligand reductions cannot be obtained as they exhibit irreversible behaviour. The reduction potentials of the complexes infer there is a similarity in the nature of the metal–ligand interaction. The variations may well be due to the different steric constraints imposed on the ligands by the bridgehead atoms as suggested by Hafeli and Keene,[25] and elucidated by the structural studies described previously.

Ab initio studies

Single-point density functional theory *ab initio* calculations at the X-ray geometries have been performed for the $[Co\{CH(C_5H_4N\text{-}2)_3\}_2]^{n+}$ and $[Co\{P(C_5H_4N\text{-}2)_3\}_2]^{n+}$ ions (n = 1–3). For comparison similar calculations were also run on the $[Co(bipy)_3]^{n+}$ (n = 1–3) system. Mulliken population analysis has been used to obtain information about the atomic charges of these complexes. Although such population-analysis schemes are sensitive to the basis set used they generally provide good comparative results across series of closely related molecules.[33,35] In this work the population analysis was employed to provide supplementary information in support of the experimental data.

Results of the DFT calculations are summarized in Table 6. Only one spin state was considered for each of the cobalt-(I) and -(III) species, formally high and low spin respectively. The ion $[Co(bipy)_3]^{2+}$ is considered to be a high-spin species, although a low-spin form can also be postulated. The high-spin form of $[Co(bipy)_3]^{2+}$, and of the tripod species, is calculated to be the more stable spin state, which is in accord with the experimental data for $[Co(bipy)_3]^{2+}$.[20] In all species investigated the calculated bond orders (Co–N overlap populations) are of a similar magnitude and no significant differences or trends are apparent. These calculations are geometry dependent; however, the results can be interpreted as indicating no major difference exists between the strength of the Co–N bonds within the different species. Significant differences do exist in the calculated spin density of the cobalt, with the cobalt(I) and high-spin cobalt(II) species having approximately equal spin density, and the low-spin cobalt(II) species having relatively less spin (as expected); the cobalt(III) species are formally spin neutral. The similarity between the spin states on the high-spin Co^{II} and Co^{I} suggests a similarity in the local cobalt electronic environments in each case that is independent of the formal oxidation state of the species. Such a conclusion could also be drawn from the fact that relatively sharp ^{1}H NMR spectra can be observed for both $[Co(bipy)_3]^{+}$ and $[Co(bipy)_3]^{2+}$.[19,61]

Mulliken atomic charges for the cobalt and nitrogen atoms are presented in Table 7. The calculated charges on the cobalt atoms are somewhat less than the formal oxidation states, indicating that the charge is distributed throughout the entire systems, consistent with a π-back bonding mechanism. It is important to note that the population analysis and partitioning of charge (and spin) onto any particular centre is not unique so that the resulting total atomic charge is *not* an exact or unique measure. A more complete analysis using fully geometry-optimized structures with high-level basis sets and an atoms in molecules (AIM) description [62] of the intramolecular charge distribution of the present complexes is being investigated.[63] What is apparent from the results presented is that the cobalt(II)–radical anion ligand species model for the cobalt(I) species is not supported by these calculations, and that the spin-density and Mulliken-analysis results suggest an equivalence between the cobalt environments within the cobalt-(I) and -(II) species.

Conclusion

Although no individual experiment reported here provides an unequivocal picture of the nature of the stabilization of the cobalt(I) oxidation state in the present complexes, the accumulation of evidence from the variety of measurements obtained presents a consistent description. The X-ray and EXAFS data are in close accord, and show the Co–N bond lengths in the order $Co^{I} \approx Co^{II} < Co^{III}$, suggesting there is a similarity in the local cobalt environment for the +I and +II oxidation states. Further analysis shows that the C–X bridgehead distance can be wholly explained as a function of the bridging atom, without reference to the oxidation state of the complex. Similar observations have also been made for the $[Co(bipy)_3]^{n+}$ system. The AOM analysis of the electronic spectra yields very similar bonding parameters for the ligands $X(C_5H_4N\text{-}2)_3$ (X = CH or P) when complexed to Co^{II}. This implies that the bridgehead

Table 6 Results of SCF calculations on the cobalt polypyridyl species

System	Charge	Multiplicity	E [a]	Co–N Overlap population [b]	Spin density on Co [c]
$[Co(bipy)_3]^{n+}$	1	3	−2838.0916	0.1927	2.67
	2	2	−2837.8077	0.1939	1.02
	2	4	−2837.8154	0.1950	2.85
	3	1	−2837.0196	0.1893	0.00
$[Co\{CH(C_5H_4N\text{-}2)_3\}_2]^{n+}$	1	3	−2914.7905	0.1871	2.31
	2	2	−2914.5705	0.1936	0.76
	2	4	−2914.5764	0.1897	2.77
	3	1	−2913.8383	0.1983	0.00
$[Co\{P(C_5H_4N\text{-}2)_3\}_2]^{n+}$	1	3	−3515.2157	0.2021	2.52
	2	2	−3515.0042	0.1927	0.96
	2	4	−3515.9491	0.1894	2.35
	3	1	−3514.6512	0.2041	0.00

[a] Electronic energy in Hartrees (≈4.36×10^{-18} J). [b] Average calculated from Mulliken population overlaps. [c] Total orbital spin condensed onto the cobalt atom; total spin multiplicity of the system = 1.

Table 7 Mulliken populations on the cobalt and nitrogen atoms of the cobalt polypyridyl species

		Charge/multiplicity			
System	Atom	1/3	2/2	2/4	3/1
$[Co(bipy)_3]^{n+}$	Co	0.884	0.907	0.937	1.451
	N	−0.646	−0.651	−0.644	−0.740
	N	−0.714	−0.721	−0.721	−0.740
	N	−0.671	−0.678	−0.679	−0.764
	N	−0.634	−0.632	−0.644	−0.749
	N	−0.650	−0.653	−0.648	−0.762
	N	−0.685	−0.682	−0.694	−0.751
$[Co\{CH(C_5H_4N\text{-}2)_3\}_2]^{n+}$	Co	0.858	0.957	0.950	1.404
	N	−0.674	−0.655	−0.660	−0.719
	N	−0.651	−0.660	−0.658	−0.715
	N	−0.672	−0.664	−0.658	−0.740
	N	−0.675	−0.655	−0.660	−0.719
	N	−0.656	−0.660	−0.656	−0.715
	N	−0.671	−0.665	−0.658	−0.740
$[Co\{P(C_5H_4N\text{-}2)_3\}_2]^{n+}$	Co	1.021	1.405	1.362	1.640
	N	−0.621	−0.633	−0.649	−0.666
	N	−0.622	−0.690	−0.696	−0.653
	N	−0.619	−0.650	−0.660	−0.663
	N	−0.639	−0.614	−0.625	−0.667
	N	−0.620	−0.679	−0.689	−0.657
	N	−0.618	−0.677	−0.672	−0.663

atom has little influence on the bonding parameters. The cobalt(I) complexes $[Co\{CH(C_5H_4N\text{-}2)_3\}_2]^+$ and $[Co\{P(C_5H_4N\text{-}2)_3\}_2]^+$ have similar bonding parameters that probably correspond to a somewhat larger ligand-field splitting than for the cobalt(II) complexes, possibly due to the influence of $Co(d_\pi)\rightarrow L(\pi^*)$ back donation. Results from the DFT calculations suggest that despite the formal oxidation state on the complexes the cobalt-(I) and -(II) species all have similar Mulliken charges and spins on the Co atom. Also, the sum of the Mulliken charges on the cobalt and co-ordinated nitrogens is ≈ −3 for the cobalt-(I) and -(II) complexes studied. This indicates that the ligand accepts a greater or lesser degree of electron density as required to maintain a stable environment around the cobalt.

Accordingly, $Co(d_\pi)\rightarrow L(\pi^*)$ back donation appears to be operative in both the present cobalt(I) complexes. However, the clear inference of the studies is that conjugation between the pyridine ligands is not a significant feature with regard to the bonding of any of these ligands with Co^{I}, and the back donation is not further stabilized by electron delocalization within the ligand system. If delocalization is to be discounted, the most likely option is simply that of the chelate effect stabilizing the high charge accumulation on the tripod ligands resulting from π-back donation. Such a conclusion, while not in fundamental disagreement with current thinking, widens the possible variety of ligand systems that may stabilize Co^{I} and therefore extend the possible catalytic actions of this metal ion.

Acknowledgements

This work was supported by the Australian Research Council (F. R. K., M. A. H., E. R. T. T. and T. W. H.). We thank the Director of the Daresbury Laboratory (UK) for the provision of facilities for the EXAFS measurements.

References

1 A. Juris, S. Barigelletti, S. Camagna, V. Balzani, P. Belser and A. von Zelewsky, *Coord. Chem. Rev.*, 1988, **84**, 85.
2 B. S. Brunschwig, C. Creutz, D. H. Macartney, T.-K. Sham and N. Sutin, *Faraday Discuss. R. Soc. Chem.*, 1982, **74**, 113.
3 C. Creutz and N. Sutin, *Coord. Chem. Rev.*, 1985, **64**, 321.
4 H. A. Schwarz, C. Creutz and N. Sutin, *Inorg. Chem.*, 1985, **24**, 433.
5 S. Margel, W. Smith and F. C. Anson, *J. Electrochem. Soc.*, 1978, **125**, 241.
6 D. J. Szalda, C. Creutz, D. Mahajan and N. Sutin, *Inorg. Chem.*, 1983, **22**, 2372.
7 C. V. Krishnan, B. S. Brunschwig, C. Creutz and N. Sutin, *J. Am. Chem. Soc.*, 1985, **107**, 2005.
8 C. V. Krishnan, C. Cruetz, D. Mahajan, H. A. Schwarz and N. Sutin, *Isr. J. Chem.*, 1982, **22**, 98.
9 C. V. Krishnan and N. Sutin, *J. Am. Chem. Soc.*, 1981, **103**, 2141.
10 F. R. Keene, C. Creutz and N. Sutin, *Coord. Chem. Rev.*, 1985, **64**, 247.
11 J. Hawecker, J.-M. Lehn and R. Ziessel, *J. Chem. Soc., Chem. Commun.*, 1983, 536.
12 J.-M. Lehn and R. Ziessel, *Proc. Natl. Acad. Sci. USA*, 1982, **79**, 701.

13 S. Margel and F. C. Anson, *J. Electrochem. Soc.*, 1978, **125**, 1232.
14 D. A. Reitsma and F. R. Keene, *Organometallics*, 1994, **13**, 1351.
15 T. Saji and S. Aoyagui, *J. Elecroanal. Chem. Interfacial Electrochem.*, 1974, **60**, 1.
16 Y. Kaizu, Y. Torii and H. Kobayashi, *Bull. Chem. Soc. Jpn.*, 1970, **43**, 3296.
17 G. M. Waind and B. Martin, *J. Inorg. Nucl. Chem.*, 1958, **8**, 551.
18 D. K. Lavallee, M. D. Baughman and M. P. Phillips, *J. Am. Chem. Soc.*, 1977, **99**, 718.
19 R. J. Fitzgerald, B. B. Hutchinson and K. Nakamoto, *Inorg. Chem.*, 1970, **9**, 2618.
20 R. W. Asmussen, *Magneto Kemiske Undersogelser over Uorganiske Kompleksforbindsler*, Gjellerups, Forland, Copenhagen, 1944.
21 D. K. Lavellee and E. B. Fleischer, *J. Am. Chem. Soc.*, 1972, **94**, 2583.
22 K. Yanagi, Y. Osashi, Y. Kaizu and H. Kobayashi, *Bull. Chem. Soc. Jpn.*, 1981, **54**, 118.
23 R. K. Boggess and D. Zatko, *Inorg. Nucl. Chem. Lett.*, 1976, **12**, 7.
24 R. K. Boggess and D. Zatko, *Inorg. Chem.*, 1976, **15**, 626.
25 T. A. Hafeli and F. R. Keene, *Aust. J. Chem.*, 1988, **41**, 1379.
26 D. D. Perrin, W. L. F. Armarego and D. R. Perrin, *Purification of Laboratory Chemicals*, Permagon, London, 1980.
27 N. Binsted, J. W. Campbell, S. J. Gurman and P. C. Stephenson, SERC Daresbury Laboratory, 1991.
28 F. R. Keene, M. R. Snow, P. J. Stephenson and E. R. T. Tiekink, *Inorg. Chem.*, 1988, **27**, 2040.
29 GAUSSIAN 94, Revision B.3, M. J. Frisch, G. W. Trucks, H. B. Schlegel, P. M. W. Gill, B. G. Johnson, M. A. Robb, J. R. Cheeseman, T. Keith, G. A. Petersson, J. A. Montgomery, K. Raghavachari, M. A. Al-Laham, V. G. Zakrzewski, J. V. Ortiz, J. B. Foresman, C. Y. Peng, P. Y. Ayala, W. Chen, M. W. Wong, J. L. Andres, E. S. Replogle, R. Gomperts, R. L. Martin, D. J. Fox, J. S. Binkley, D. J. Defrees, J. Baker, J. P. Stewart, M. Head-Gordon, C. Gonzalez and J. A. Pople, Gaussian Inc., Pittsburgh, PA, 1995.
30 S. H. Vosko, L. Wilk and M. Nusair, *Can. J. Phys.*, 1980, **58**, 1200.
31 R. S. Mulliken, *J. Chem. Phys.*, 1955, **23**, 2338.
32 R. S. Mulliken, *J. Chem. Phys.*, 1955, **23**, 1833.
33 W. J. Hehre, L. Radom, P. v. R. Schleyer and J. A. Pople, *Ab Initio Molecular Orbital Theory*, Wiley, New York, 1986.
34 M. Vitale, C. K. Ryu, W. E. Palke and P. C. Ford, *Inorg. Chem.*, 1994, **33**, 561.
35 G. S. Chandler, G. A. Christos, B. N. Figgis, D. P. Gribble and P. A. Reynolds, *J. Chem. Soc., Faraday Trans*, 1992, 1953.
36 G. M. Sheldrick, in *Crystallographic Computing 3*, eds. G. M. Sheldrick, C. Krüger and R. Goddard, Oxford University Press, Oxford, 1986, pp. 175–189.
37 D. T. Cromer and J. T. Waber, *International Tables for X-Ray Crystallography*, Kynoch Press, Birmingham, 1974, vol. 4, pp. 2339–2346.
38 J. A. Ibers and W. C. Hamilton, *Acta Crystallogr.*, 1964, **17**, 781.
39 D. C. Creagh and W. J. McAuley, in *International Tables for Crystallography*, ed. A. J. C. Wilson, Kluwer Academic Publishers, Boston, 1992, vol. C, Table 4.2.6.8, pp. 219–222.
40 D. C. Creagh and J. H. Hubbell, in *International Tables for Crystallography*, ed. A. J. C. Wilson, Kluwer Academic Publishers, Boston, 1992, vol. C, Table 4.2.4.3, pp. 200–206.
41 TEXSAN, Crystal Sructure Analysis Package, Molecular Structure Corporation, Houston, TX, 1985 and 1992.
42 C. K. Johnson, ORTEP, A Thermal Ellipsoid Plotting Program, Oak Ridge National Laboratory, Oak Ridge, TN, 1965.
43 N. Walker and D. Stuart, *Acta Crystallogr., Sect. A*, 1983, **39**, 158.
44 G. M. Sheldrick, SHELX 76, *Program for Crystal Structure Determination*, Univeristy of Cambridge, 1976.
45 E. S. Kucharski, W. R. McWhinnie and A. H. White, *Aust. J. Chem.*, 1978, **311**, 2647.
46 D. A. Szalda and F. R. Keene, *Inorg. Chem.*, 1986, **25**, 2795.
47 T. Astley, J. M. Gulbis, M. A. Hitchman and E. R. T. Tiekink, *J. Chem. Soc., Dalton Trans.*, 1993, 509.
48 R. Taylor and F. H. Allen, *Structure Correlation*, eds. H.-B. Bürgi and J. D. Dunitz, VCH, Weinheim, 1994, vol. 4, pp. 111–161.
49 P. A. Lee and J. B. Pendry, *Phys. Rev. B*, 1975, **11**, 2795.
50 B. K. Teo, *EXAFS: Basic Principles and Data Analysis*, Springer, Berlin, 1986.
51 S. J. Gurman, N. Binsted and I. Ross, *J. Phys. C.*, 1986, **19**, 1845.
52 S. J. Gurman, N. Binsted and I. Ross, *J. Phys. C.*, 1984, **17**, 143.
53 C. D. Garner, *Adv. Inorg. Chem.*, 1991, **36**, 303.
54 T. Astley, A. J. Canty, M. A. Hitchman, G. L. Rowbottom, B. W. Skelton and A. H. White, *J. Chem. Soc., Dalton Trans.*, 1991, 1981.
55 A. B. P. Lever, *Inorganic Electronic Spectroscopy*, Elsevier, Amsterdam, 1984, p. 480.
56 E. Larsen, G. N. La Mar, B. E. Wagner, J. E. Parks and R. H. Holm, *Inorg. Chem.*, 1972, **11**, 2652.
57 T. Astley, Ph.D. Thesis, University of Tasmania, 1993.
58 T. Astley, M. A. Hitchman, F. R. Keene and E. R. T. Tiekink, *J. Chem. Soc., Dalton Trans.*, 1996, 1845.
59 B. N. Figgis, *Introduction to Ligand Fields*, Interscience, New York, 1964, p. 52.
60 M. A Hitchman, *Inorg. Chem.*, 1982, **21**, 821.
61 M. L. Wicholas and R. S. Drago, *J. Am. Chem. Soc.*, 1968, **90**, 2196.
62 R. F. W. Bader, *Atoms in Molecules, A Quantum Theory*, Clarendon, Oxford, 1990.
63 K. R. Adam, I. M. Atkinson, N. Green and F. R. Keene, unpublished work.

Received 29*th August* 1996; *Paper* 6/05967H